Micro/Nanometer-Scale Fiber with Highly Ordered Structures by Mimicking the Spinning Process of Silkworm

*Su-Kyoung Chae, Edward Kang, Ali Khademhosseini, and Sang-Hoon Lee**

Silkworm silk, produced by *Bombyx mori*, has been extensively used for 5000 years in the textile industry.[1] Recently, *B. mori* silk has attracted the attention of scientists and engineers owing to its diverse applications in textile, optical, and biomedical fields.[2–4] To generate silk fiber materials, diverse artificial spinning methods, such as solvent extrusion, electrospinning, and microfluidic approaches, have been developed. For example, regenerated silk from *B. mori* silkworms was extruded into fibers from an ionic liquid solvent system.[5] The formation of electrospun fibers from aqueous *B. mori* silkworm silk solution or with polymer was reported.[6,7] A microfluidic chip was used for the concentration of regenerated silk fibroin aqueous solution by biomimicking the silk glands and the spinning duct of silkworms.[8] However, it was impossible to reduce the width of the biopolymer to nanometer-scale dimensions and to produce multiple fibers with different sizes in a single microchannel. Moreover, there is a lack of a molecular structural transition on the artificial fibers in such systems and this technique is still a challenge during the spinning process.

Silk fiber is made of two different proteins–the core structural protein called fibroin and the gummy sheath protein called sericin.[9] **Figure 1**a is a schematic of the spinning duct of the silkworm. The main structural silk protein fibroin is synthesized at the epithelial wall of the posterior segment. Next, the fibroin moves forward in the wider middle division, where the concentration of fibroin protein increases and aggregation of micelle-like particles (100–200 nm in diameter) inducing the formation of globules of a size of 0.8 to 15 μm diameter begins.[10] Shearing or elongation of this phase in the narrow duct cause the orientation and stretching of the globules. Finally, crystallization of *B. mori* silk occurs under shear stress and dehydration conditions. During spinning, the water content decreases from 88 to 70% from the posterior division to the anterior division in the gland.[11]

Here we focused on the crystalline structure of the proteins as a result of the dehydration of the aqueous phase and shear stress. Researchers have reported that β-sheet crystals that are formed by means of hydrogen bonds and the configuration of molecules by solvent exposure play a key role in defining the mechanical properties of silk.[12,13] Such an ordered structure of molecules is an important factor for improving the physical properties of fibers. A regenerated silk fibroin mat of highly crystalline structure displaying outstanding mechanical strength has been reported.[13] In this paper, organic solvents such as methanol have been shown to affect the crystallization by inducing a random coil to β-sheet transition.[14,15] Dehydration changes the conformation of silk protein domains to crystalline sheets with hydrogen bonds providing strength and stability.[16] Therefore, as the silk fibroin is immersed in a dehydrating solvent such as methanol, crystallization is induced as the silk fibroin chains undergo a transformation from a random-coil to β-sheet conformation.[17] In contrast, water disrupts the hydrogen bonds between chain segments in the amorphous phase. As a result, the immersion of silk proteins in water decreases the mechanical properties of silk.[18]

Inspired by such a crystalline structure, obtained by means of hydrogen bonding due to dehydration and physical shear, forming the basis for the mechanical strength of silk proteins in the silkworm spinning mechanism, we introduce a novel spinning method to create ultrathin, crystal-like ordered, and multiple polymeric fibers within a single microfluidic system, challenging previous spinning methods. It is recognized that ionic polymers in solvents of low polarity tend to aggregate due to the attractive force of the ionic dipoles.[19] Isopropyl alcohol (IPA) has a weaker polarity (3.9) than water (9.0).[20] Therefore the aggregation behavior of polymer chains can be induced with IPA treatment.

By utilizing a microfluidic spinning method that mimics the spinning mechanism of the silk worm, alginate fibers of a highly ordered structure were fabricated. Microfluidic chips are popularly used to modulate the physiochemical property of microscale fibers or particles.[21–27] A highly ordered structure with numerous nanostrands was generated by dipole–dipole attractions at the dehydrating interface between the aqueous polar core and IPA sheath fluid. The shear force in the microfluidic channel enables the alignment of polymer chains to form a compact structure, which enabled the size of the fiber to be reduced to as low as a few tens of nanometers thick. Scanning electron microscopy (SEM) and transmission electron

Dr. S.-K. Chae, E. Kang, Prof. S. H. Lee
Department of Biomedical Engineering
College of Health Science
Korea University
Jeongeung-dong, Seongbuk-gu, Seoul,
136-703, Republic of Korea
E-mail: dbiomed@korea.ac.kr
Dr. A. Khademhosseini
Center for Biomedical Engineering
Department of Medicine
Brigham and Women's Hospital
Harvard Medical School, Cambridge, Massachusetts 02139, USA
Dr. A. Khademhosseini
Harvard-MIT Division of Health Sciences and Technology
Massachusetts Institute of Technology
Cambridge, Massachusetts 02139, USA
Dr. A. Khademhosseini
Wyss Institute for Biologically Inspired Engineering
Harvard University
Boston, Massachusetts 02115, USA

DOI: 10.1002/adma.201300837

ADVANCED MATERIALS
www.advmat.de

www.MaterialsViews.com

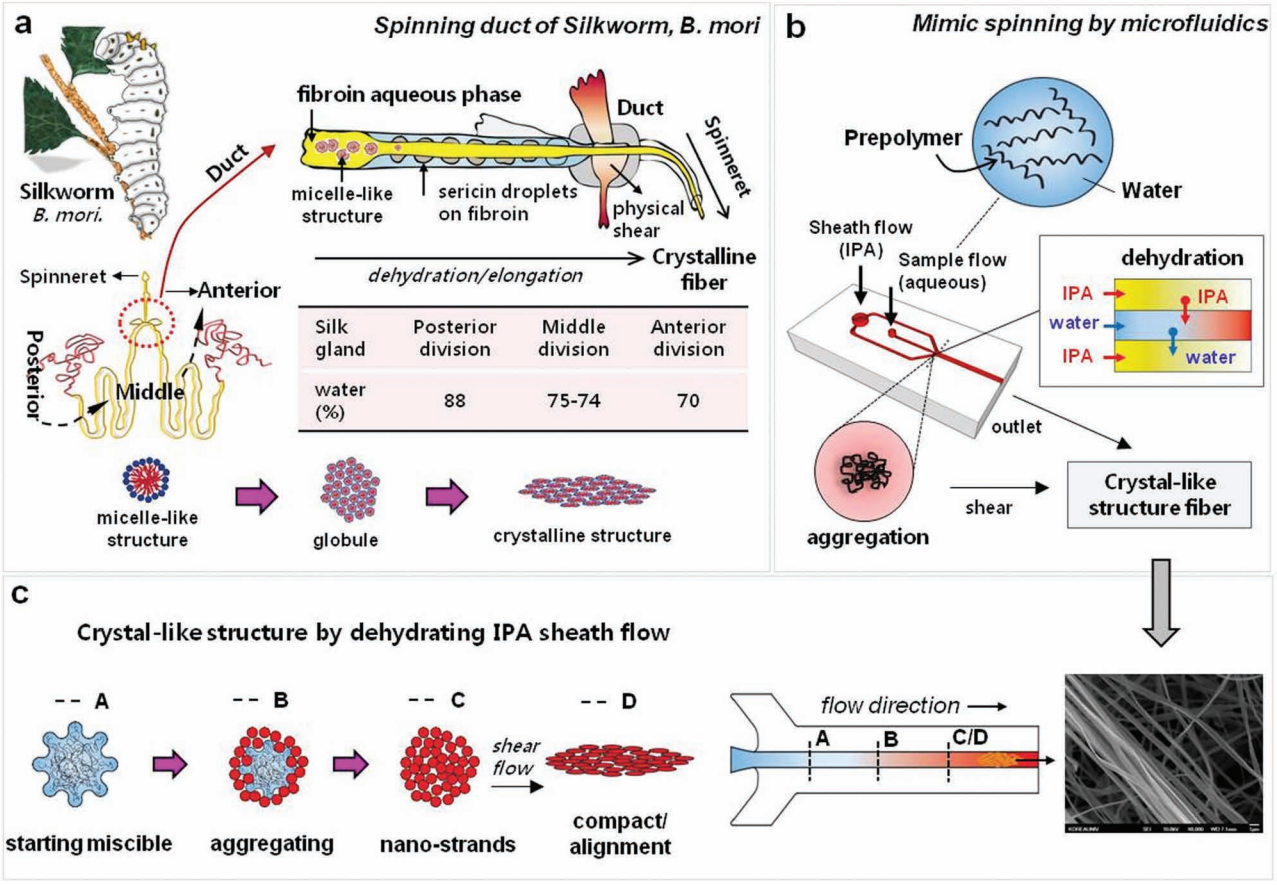

Figure 1. Schematic of the formation of self-aggregated fibers using isopropyl alcohol (IPA) sheath flow. a) Illustration of a silkworm's duct spinning. b) Microfluidic system consisting of two inlet channels and one outlet channel, with aqueous alginate and IPA used as the core and sheath flow. c) Dehydration process of aqueous alginate with IPA solvent under chemical focusing and physical shear in a microchannel.

microscopy (TEM) analysis revealed that the nanostrands were highly aligned along the direction of the flow. FT-IR analysis revealed a stronger hydrogen bond in IPA-based fibers than that in water-based fibers. The X-ray diffraction (XRD) pattern of an IPA-based fiber showed a strong and sharp peak. From these results we suggest that more highly ordered fibers can be fabricated through dehydration and physical shear within the microfluidic system.

Our method enables the polymer chains in the fibers to self-align along the direction of flow to form crystal-like ordered structures, with widths that varied from 70 nm to 20 μm. The results also demonstrate that diverse fiber shapes can be prepared by just controlling the flow rate.

In addition, the proposed method can be used to generate multiple fibers with different widths simultaneously without the need of additional apparatus or treatments. At the dehydrating interface between core and sheath fluids, induction of Kelvin–Helmholtz instabilities yielded the simultaneous production of multiple nanometer and micrometer-scale fibers that could not be produced by conventional microfluidic spinning methods. The microfluidic spinning method is a unique method to control the size, shape, and material composition of single or multiple micro and nanometer-scale fibers and will attract much attention of researchers in the fields of tissue engineering, biomedical engineering, and the textile industry.

Our fiber spinning microfluidic system consisted of two inlet and one outlet channels (Figure 1b). The width of the main channel was focused from an initial width of 100 μm to an intersection point with a width of 30 μm and a height of 100 μm (Figure S1, Supporting Information). Spinning was accomplished by introducing a dilute aqueous solution of alginate (<1%) and IPA solvent as the core and sheath fluids. An alginate prepolymer solution dispersed in water was injected into the microchannel. The prepolymer core stream was surrounded by water-miscible IPA solvent at the junction. As dehydration by the IPA sheath flow gradually progressed toward the aqueous core phase, polymer chains in the core flow self-aggregated. Shear force was simultaneously applied to this state, similar to the silkworm spinning process, and a crystal-like ordered fiber with aligned nano-strands was created. Figure 1c illustrates the procedure by dehydrating IPA solvent to generate high-ordered structures with compact alignment. The core solution started dehydration with the IPA sheath phase (line A in Figure 1c), and alginate chains were self-aggregated due to an IPA solvent-resistant micelle-like structure (line B in Figure 1b). The self-aggregated chains formed densely packed

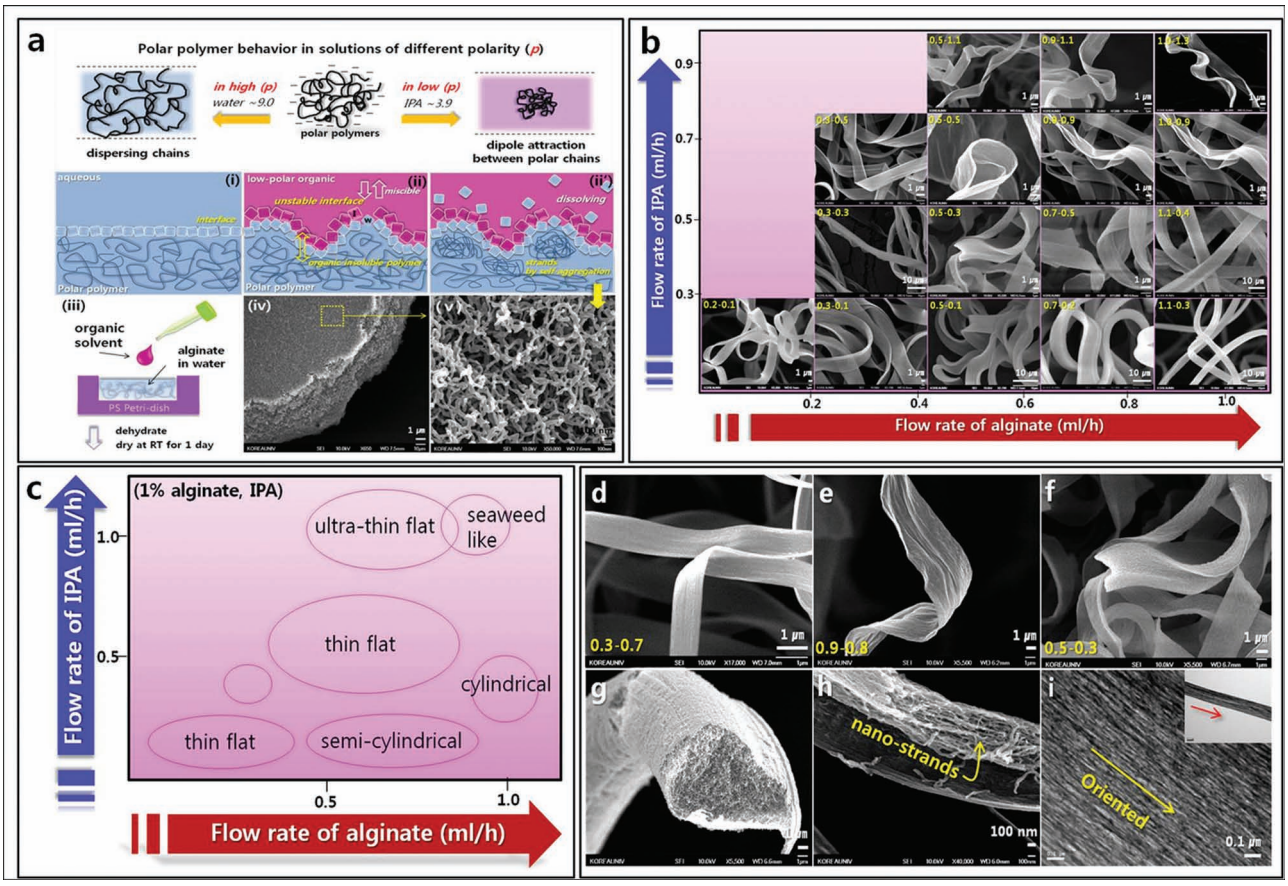

Figure 2. Alginate fibers made by using IPA within the microchannel: a) Polar polymer behavior in solutions of different polarity (*p*); i) the behavior of the alginate polymer chains at the interface between the aqueous–aqueous, and ii,ii') polar aqueous–low polar organic system; iii) process of self-aggregation of the polymer chains in the presence of the IPA solution; iv) SEM images of the solidified alginate structures; v) high magnification image of (iv). The strand width is approximately 40 nm. b) SEM images of the alginate fibers prepared over a wide range of flow rates. The numerical labels in each image indicate the flow rate (alginate–IPA, mL h^{-1}). c) The fiber shapes were categorized according to: d) thin flat, e) seaweed-like structures, f) semi-cylindrical, and g) cylindrical. h) Side view of a cylindrical fiber. i) TEM image of a flat fiber. Scale bar is 0.1 μm.

nanostrands (line C in Figure 1c), and the shear force inside the microfluidic channel helped in closely packing the fibers (line D in Figure 1c) similar to the crystalline structure in the spinning duct of silkworms. Finally, the alginate fibers with diverse widths ranging from thin (<10 μm) to ultrathin (<100 nm) were successfully generated.

To prove this mechanism, we first investigated the creation of nanostrands from polymer self-aggregation. We hypothesized that self-aggregated strands could be induced by the dipole attraction when polar polymer chains are dehydrated with a low-polarity solvent (**Figure 2**a). When an aqueous solution containing polar polymer contacts a solution of similar polarity, it is diluted without affecting the motion of the polymer chains (Figure 2a(i)). On the other hand, as the aqueous solution is exposed to a weakly polar organic solvent, the polymer chains at the dehydrating interface begin to self-aggregate (Figure 2a(ii-ii')).

To test such aggregation behavior experimentally, we tested a number of water-soluble polar molecules including poly(vinyl alcohol) (PVA), gelatin, and alginate. As seen in the SEM images of Figure S2, Supporting Information, all polymer chains were self-aggregated. Among these polar molecules, alginate was selected as the model polymer as it forms well-organized porous structures with numerous nanostrands and is widely used as a biomaterial, with Food and Drug Administration (FDA) approval for a number of applications. The aggregation behavior of alginate in solvents with diverse polarities was investigated using methanol, ethanol, and IPA, all of which are water-miscible organic solvents with low polarities of 3.9 (IPA), 4.3 (ethanol), and 5.1 (methanol) (Figure S3, Supporting Information).[20,28] A 5 mL aliquot of each organic solvent was added dropwise to 200 μL samples of aqueous alginate solution, as shown in Figure 2a (iii). The alginate immediately self-aggregated, creating numerous strands, which formed large solid polymer structures. SEM observation revealed that the alginate exposed to IPA clearly showed a more porous morphology than that exposed to the other solvents (Figure 2a(iv)). These results demonstrate that the aggregation behavior depended on the polarity of the solvents. In the high-resolution SEM image in Figure 2a(v), the self-aggregated alginate consists of numerous nanostrands with a diameter of approximately 40 nm (Figure S4, Supporting Information).

These regular nanostrands began to form highly ordered structures, which resemble the fibroin aggregation process in the spinning mechanism of silkworm silk. Fibroin globules are aligned with increasing applied shear to the crystalline structure. To mimic this process, polymer chains were self-aggregated and subsequently exposed to hydrodynamic shear. They were spun over a wide range of shear rates by using a continuous flow microfluidic system. For these experiments, 1% aqueous alginate and 0.05% $CaCl_2$ in IPA solution were used as a core and sheath flow.

Figure 2b demonstrates SEM images of fibers with diverse shapes as a function of flow rate. The core streams were easily deformed according to the balance of core and sheath flow rates due to the low interfacial tension.[29,30] A cross-sectional schematic of the deformation process in the core stream is shown in Figure S5, Supporting Information. At low flow rates, the aqueous alginate phase in contact with IPA was horizontally elongated in its cross-section and vertically flat (Type I in Figure S5), whereas at high flow rates, the alginate phase was elongated in the vertical direction due to the lateral flow strength (Type III in Figure S5). At a balanced flow rate, a cylindrical core stream was formed (Type II in Figure S5). The cross-sectional shapes of the fibers can be categorized according to the flow rates of the two liquids (Figure 2c), as thin sheets (low core–low sheath, Figure 2d), seaweed-like (high core–high sheath, Figure 2e), semi-cylindrical (middle core–low sheath, Figure 2f), and cylindrical (high core–low sheath) (Figure 2g). Cylindrical fibers were generated over a limited range of flow rates (1.1 ± 0.2 mL h^{-1} (core) and 0.3 ± 0.2 mL h^{-1} (sheath)). Figure 2g shows a cross-sectional image of the cylindrical fiber, demonstrating that a fiber consists of numerous aligned strand bundles. A side-view of a cylindrical fiber is shown in Figure 2h, where the nanostrands in the fiber structure can be seen to be well-aligned and oriented parallel to the direction of flow.[31] The high degree of alignment and the directionality of the strands in a fiber is clearly visible in the TEM image in Figure 2i, with strands of less than 10 nm in diameter. The width of a single alginate chain is known to be between 1.41 and 4.65 nm;[32] therefore, the aligned lines visible in the TEM image may represent the alignment of alginate polymer chains formed under the shear flow. Flow rate determined the competition between the aggregation behavior due to chemical dehydration and elongation due to physical shear in the resulting products. In the case of flat fibers, there was obvious alignment by the elongation. At low IPA sheath flow, the cylinder type could be formed because aggregation behavior was stronger than elongation flow. This is similar to the protein assembly and alignment due to shear in the silkworm spinning.

To investigate the effect of IPA sheath flow on the fiber structure of ordered nanostrands, alginate fiber from IPA-based sheath flow was compared with that of water-based sheath flow. In these comparisons, 0.05% $CaCl_2$ in IPA and 0.05% $CaCl_2$ in water were used as the sheath flows. The inner structure of each fiber was analyzed by XRD, FT-IR spectroscopy, and inductively coupled plasma–optical emission spectroscopy (ICP-OES). In addition, the relative amounts of Ca^{2+} ions in the fiber structures were analyzed using ICP-OES. The amount of Ca^{2+} incorporated into each fiber, as determined using ICP-OES,[33] is listed in Table 1(S2) in the Supporting Information. We found that the amount of Ca^{2+} in the fibers prepared using IPA was nearly twice that in the fibers prepared using water. **Figure 3**a shows the XRD patterns of fibers produced using IPA-based (red line) and water-based (blue line) sheath fluid. The pattern in the IPA-based sheath flow result is similar to the crystalline structure of fibroin in the fibroin porous sponge.[34] Two peaks are observed at around 2θ 16.50 and 23.80 in the spectra in both conditions, however, in the case of IPA-based sheath flow, the peak intensity at 2θ 23.80 is much stronger than that observed in the pattern of water-based sheath flow. The strengths of 2θ in the spectra reflect the crystalline degree. The sharp peaks demonstrate the chain alignment, corresponding to diffraction from oriented polymer chains. Thus, we suggest that the solvent system induces conformational changes, leading to an ordered structure due to dehydration.[35]

FT-IR analysis revealed that a stronger hydrogen bond occurred between chains of IPA-based fibers from the shift and shape of bands (Figure S6, Supporting Information). In the water-based fiber FT-IR spectrum there are two bands due to the hydrogen bound –COO group at 1603 (asymmetric) and 1445 cm^{s-1} (symmetric).[36] The bending vibration of water also appears at about 1625 cm^{-1} (this band disappeared in the IPA-based fiber spectrum). In the spectrum of the alginate fiber formed using IPA-based sheath flow, the bands appearing at 1595 and 1425 cm^{-1} belong to the asymmetric and symmetric –COO stretching vibrations. Compared to the water-based fiber the –COO stretching vibrations bands were shifted toward lower wavenumbers, indicating a stronger hydrogen bond between chains. The band located around 3420 cm^{-1} was caused by OH stretching and inter- and intramolecular hydrogen bonds. The OH band of the IPA-based fibers are broadened and smoothed, with a shift to lower wavenumbers, although the peak doesn't show a strong intensity. This broad feature has been attributed to the ionic interaction between ions and the OH groups or formation of intramolecular hydrogen bonds.[37] The shift is mainly due to the rearrangement of hydrogen bonds.[38] The above results supported that the OH stretching due to the intra- and intermolecular hydrogen bond was strengthened. This result was similar to that of fibroin. As fibroin is treated with a dehydrating solvent, crystallization is induced as the silk fibroin chains undergo a transformation from a random-coil to a β-sheet conformation.[14,15] Dehydration resulted in the transformation of fibroin into crystalline sheets with hydrogen bonds providing strength and stability. Therefore, the above results suggest that the resulting products from IPA sheath flow were a more highly ordered crystal-like structure than that from water sheath flow.

Next, we examined the effect of the calcium as a crosslinking agent in the structure of nanostrands. IPA solution with and without calcium ions was applied as a sheath flow. First, the fibers were fabricated using pure IPA without calcium ions as the sheath fluid, with subsequent crosslinking achieved by dipping the formed material into the crosslinking agent (sheath **1**). The second involved calcium ions in the IPA sheath fluid, causing self-aggregation and crosslinking to occur simultaneously (sheath **2**). The size of fibers produced by sheath **1** and **2** with different alginate concentrations were compared, and the results are plotted in Figure 3b. Alginate solutions containing 0.1%, 0.5%, 1.0%, or 2.0% alginate were tested, with pure IPA and 0.5% $CaCl_2$ dissolved in the IPA. The flow rates

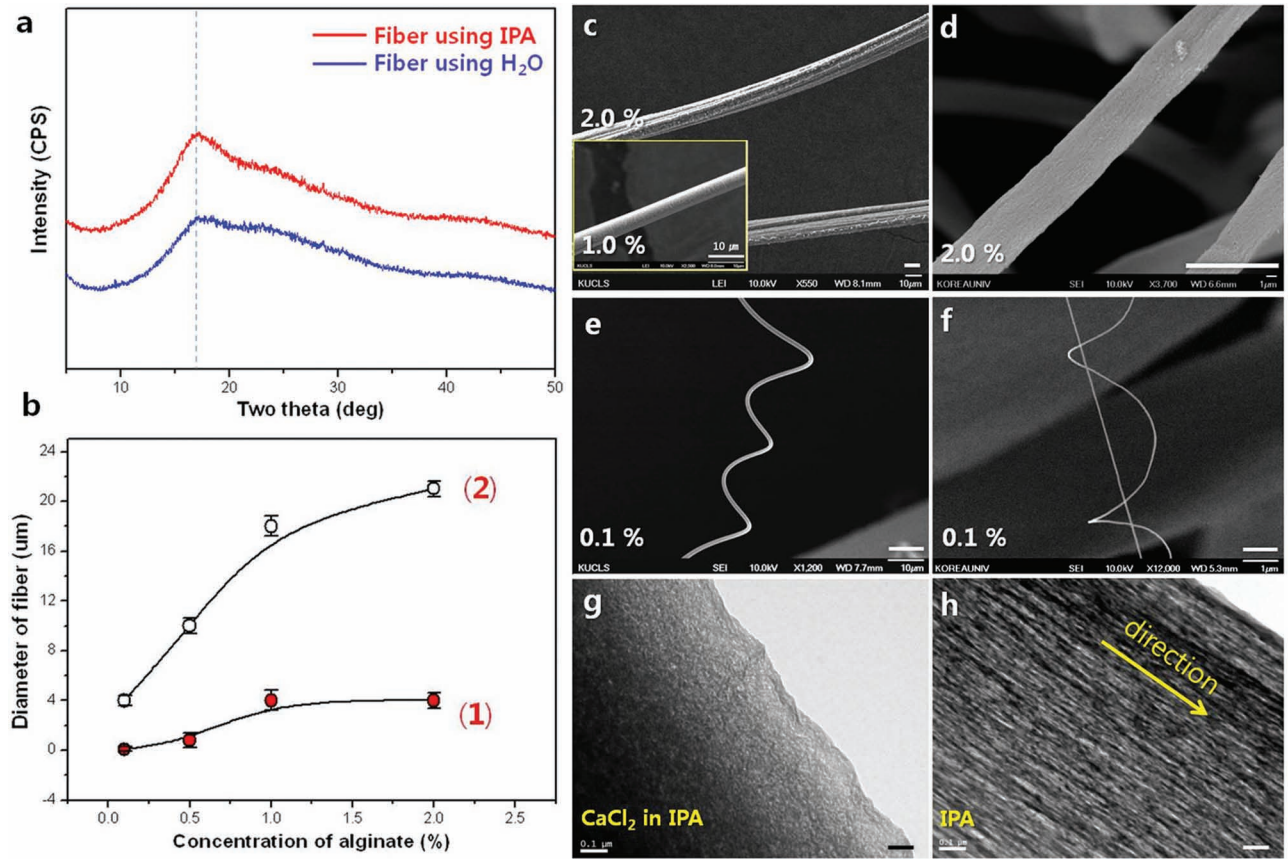

Figure 3. Characterization of alginate fibers formed by different core and sheath flow conditions. a) XRD patterns of alginate fibers using an IPA-based $CaCl_2$ solution (red line) and a water-based $CaCl_2$ solution (blue line). b) Size distribution of fibers prepared using pure IPA (**1**) or $CaCl_2$ in IPA (**2**) as the sheath fluid. SEM images of 2% alginate: c) from 0.05% $CaCl_2$ in IPA as the sheath fluid and d) from pure IPA as the sheath fluid. SEM images of 0.1% alginate: e) from 0.05% $CaCl_2$ in IPA as the sheath fluid and f) from pure IPA as the sheath fluid. TEM images of alginate fiber using: g) 2% $CaCl_2$ in IPA and h) pure IPA as the sheath flow. c–e) Scale bar is 10 μm. f) Scale bar is 1 μm. g,h) Scale bar is 0.1 μm.

of the core and sheath fluids were approximately 1.1 ± 0.2 and 0.3 ± 0.2 mL h^{-1}, respectively. The fiber size and morphology depended both on the crosslinking method and the concentration of alginate. The width of the fibers formed using sheath **2** ranged from 4 to 22 μm as the concentration of the alginate solution increased (empty rounds in Figure 3b), and the surface of the fibers were seen to be smooth from 1.0% (inset of Figure 3c) to 0.1% (Figure 3e) alginate solutions. The 2% alginate solution yielded a rough surface with parallel wrinkle patterns (Figure 3c). In contrast, the width of the fibers prepared using sheath **1** ranged from 70 nm to 4 μm, with increasing alginate concentrations (solid rounds in Figure 3b). Figure 3d and 3f show SEM images of fiber structures prepared from 2.0% and 0.1% alginate core fluids. The fiber diameters were significantly smaller at the lower concentration to approximately 70 nm. The surface morphology of a 1% alginate fiber from sheath **1** and **2** was observed by TEM. There was no specific direction in the case of sheath **2** (Figure 3g). In sheath **2**, the fibers are simultaneously aggregated and crosslinked, which may prevent dense aggregation; the fibers from this sheath flow would thus be expected to produce a larger size. By contrast, for sheath **1**, the alignment and the directionality of the strands is clearly illustrated in the TEM image (Figure 3h). The direction of the nanostrands was maintained at this moment regardless of post-crosslink (Figure S7, Supporting Information).

This is similar to the spinning process of silkworm silk where the fibroin filaments were aligned linearly and fixed as a bundle with sericin gum.[39] Similarly, by using sheath **1**, the polymer chains ordered to form the fibers and were subsequently crosslinked. But if left uncrosslinked, the flow instability conditions can be easily induced at dehydrating interfaces between core and sheath flow.

Here, by taking advantage of Kelvin–Helmholtz instabilities that occur at disturbed interfaces between miscible fluids with different densities and velocities,[40,41] we have demonstrated that the desired multi-scale fibers could be generated in a single microchannel. The instability conditions governing Kelvin–Helmholtz instabilities can be expressed as a function of the interfacial tension:

$$(U1 - U2)2 > 2\sqrt{g\sigma\left(\rho 1 - \rho 2(\rho 1 + \rho 2)\left(\frac{1}{\rho 1 \rho 2}\right)\right)} \quad (1)$$

where, ρ_1, ρ_2, U_1, and U_2 are the densities and velocities of liquids 1 and 2, g is the acceleration due to gravity, and σ is the interfacial tension between the two fluids. In our aqueous–IPA

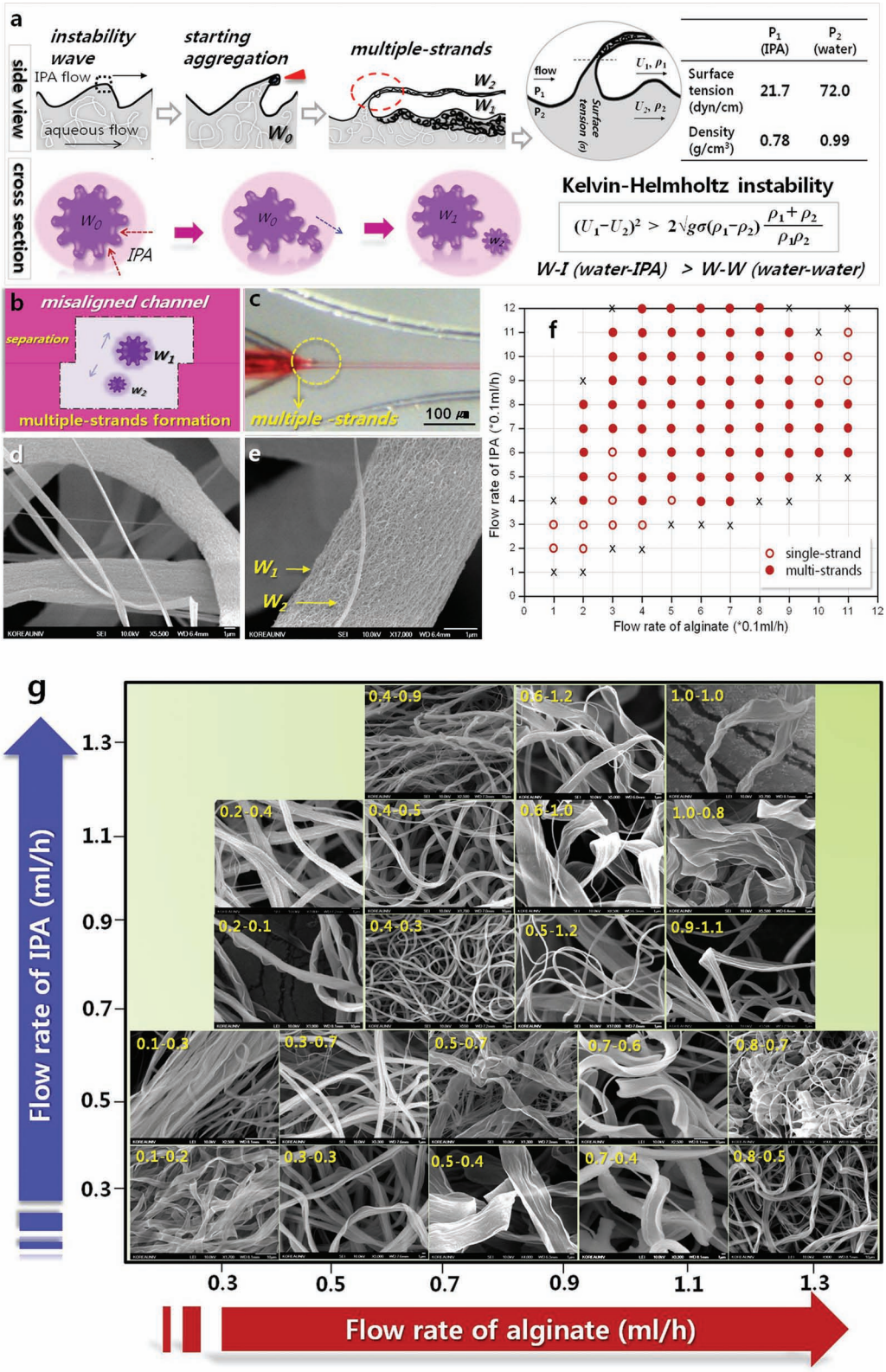

Figure 4. Principles and resulting structures of multiple fibers. a) Schematic diagram illustrating the generation of the multiple streams using an aqueous alginate–IPA system under Kelvin–Helmholtz instabilities. b) Schematic diagram showing the misaligned PDMS microchannel used for multiple strand formation. c) Two core fluid streams formed to yield multiple strands in the misaligned microchannel. d,e) SEM images of multiple alginate fibers generated using an IPA sheath fluid. f) Graph indicating the formation of multiple fibers as a function of the flow rate. g) Morphology of the multiple fibers as a function of the flow rate. The numerical label in each SEM image indicates the flow rate (alginate–IPA, mL h^{-1}).

system, the interface is especially unstable due to the strong miscibility of the two fluids, with the amplitude of the instability wave potentially becoming sufficiently large as to create separated flows. A schematic diagram for generating satellite flows using a Kelvin–Helmholtz instability wave is shown in **Figure 4**a. The side-view shows that a disturbance induces a seed wave at the interface between the two fluids that can become large (dotted black line). The core alginate flow then begins to separate at the maximum of the instability wave, and the alginate chains in the separated flow areas then self-aggregate in the IPA sheath fluid (red triangle in Figure 4a) and do not fuse downstream. In contrast, a water sheath flow does not induce the formation of a satellite stream under the instability because the high interfacial tension between the core (water) and sheath (water) fluids is relatively stable in the laminar flow (Figure S8, Supporting Information). This approach was verified by generating a disturbance in the microfluidic channel. We fabricated a microchannel that was misaligned by approximately 25% (Figure 4b and Figure S9, Supporting Information). A 1% aqueous alginate solution was introduced as the core fluid and IPA was used as the sheath fluid. At the intersection of the core and sheath flows, two streams were created because of interface instability between the aqueous and IPA liquids (Figure 4c). Figure 4d shows SEM images of multiple-stranded alginate fibers from a misaligned polydimethylsiloxane (PDMS) microchannel. Figure 4e shows that the diameters of the larger (W_1) and smaller (W_2) fibers were 3 μm and 70 nm, respectively. The graph in Figure 4f presents data obtained on multiple alginate fiber formation as a function of the flow rate within the misaligned microchannel, and demonstrates that multiple fibers could be created over a broad range of flows. The morphologies of the multiple alginate fibers prepared under each flow rate are shown in Figure 4g. As with the formation of a single fiber (Figure 2b), diverse fiber shapes were observed, including ultrathin (low flow rate), semi-cylindrical (middle), and seaweed-like structures (high). At a low initial flow rate (0.2 mL h^{-1}) and a high flow rate (exceeding 1.0 mL h^{-1}), ultrathin flat fibers were formed.

In summary, we propose a new method for the microfluidic spinning of ultrathin fibers with a highly ordered structure of nanostrands due to dehydration and physical shear by mimicking the process of the crystalline structure of *Bombyx mori* silk protein. Like the spinning of silkworm silk, the polymer chains were aligned along the flow direction by the shear force. Such an ordered structure may enable the continuous and stable generation of 70 nm wide pure alginate fibers. Furthermore, multiple fibers with different sizes could be simultaneously produced in a single channel by the instability at the dehydrating interface. Our system will provide a new technology for generating diverse functional micro and nanometer-scale fibers by combining advanced microfluidic technologies and will increase the applications, which was difficult to accomplish by conventional electrospinning or microfluidic methods.

Experimental Section

Alginate fibers were produced using a core solution of 1% w/v sodium alginate in water (Sigma, St. Louis, MO, USA), and a sheath fluid of either pure IPA or IPA containing 0.5% or 2% w/v $CaCl_2{\cdot}2H_2O$ (Sigma, St. Louis, MO USA). Microfluidic chips were fabricated using aSU8 photoresist-patterned silicon wafer as a mold. PDMS pre-polymer and crosslinker (Sylgard 184, Dow Corning) were mixed in a 10:1 ratio, poured onto the mold, and cured at 80 °C for 20 min. The PDMS substrates were then bonded together using plasma treatment. The prepared devices were kept in an oven at 80 °C for 1 day to recover their hydrophobic surface properties.

Supporting Information

Supporting Information is available from the Wiley Online Library or from the author.

Acknowledgements

This study was supported by the National Research Foundation of Korea (NRF) grant funded by the Korea government (MEST) (2012026340) and the Conversing Research Center Program through the National Research Foundation of Korea (NRF) funded by the Ministry of Education, Science and Technology (No. 2012K001360).

Received: February 22, 2013
Revised: March 18, 2013
Published online: April 25, 2013

[1] S. Sukigara, M. Gandhi, J. Ayutsede, M. Micklus, F. Ko, *Polymer* **2003**, *44*, 5721.
[2] T. Toshiki, T. Chantal, R. Corinne, K. Toshio, A. Eappen, K. Mari, K. Natuo, T. Jean-Luc, M. Bernard, C. Gerard, S. Paul, F. Malcolm, P. Jean-Claude, C. Pierre, *Nat. Biotechnol.* **2000**, *18*, 81.
[3] G. H. Altman, F. Diaz, C. Jakuba, T. Calabro, R. L. Horan, J. Chen, H. Lu, J. Richmond, D. L. Kaplan, *Biomaterials* **2003**, *24*, 401.
[4] L. W. Tien, E. S. Gil, S. Park, B. B. Mandal, D. L. Kaplan, *Macromol. Biosci.* **2012**, *12*, 1671.
[5] D. M. Phillips, L. F. Drummy, R. R. Naik, H. C. De Long, D. M. Fox, P. C. Trulove, R. A. Mantz, *J. Mater. Chem.* **2005**, *15*, 4206.
[6] H. J. Jin, J. Chen, V. Karageorgiou, G. H. Altman, D. L. Kaplan, *Biomaterials* **2004**, *25*, 1039.
[7] H. J. Jin, S. V. Fridrikh, G. C. Rutledge, D. L. Kaplan, *Biomacromolecules* **2002**, *3*, 1233.
[8] J. Luo, Y. Zhang, Y. Huang, H. Shao, X. Hu, *Sens. Actuators B* **2012**, *162*, 435.
[9] G. Takuma, I. Tamio, L. Hans, *Insect Biochem.* **1977**, *7*, 285.
[10] Y. He, N. Zhang, W. Li, N. Jia, B. Chen, K. Zhou, J. Zhang, Y. Chen, C. Zhou, *J. Mol. Biol.* **2012**, *418*, 197.
[11] J. Zhu, Y. Zhang, H. Shao, X. Hu, *Polymer* **2008**, *49*, 2880.
[12] T. E. Attwood, T. King, V. J. Leslie, J. B. Rose, *Polymer* **1977**, *18*, 369.
[13] R. Nazarov, H. J. Jin, D. L. Kaplan, *Biomacromolecules* **2004**, *5*, 718.
[14] S. Keten, Z. Xu, B. Ihle, M. J. Buehler, *Nat. Mater.* **2010**, *9*, 359.
[15] M. Tsukada, G. Freddi, P. Monti, A. Bertoluzza, N. Kasai, *J. Polym. Sci., Part B: Polym. Phys.* **2003**, *23*, 1995.
[16] T. Sumitomo, H. Kakisawa, *J. Mater. Res.* **2008**, *23*, 1466.
[17] J. Perez-Rigueiro, C. Viney, J. Llorca, M. Elices, *Polymer* **2000**, *41*, 8433.
[18] S. Lu, X. Wang, Q. Lu, X. Zhang, J. A. Kluge, N. Uppal, F. Omenetto, D. L. Kaplan, *Biomacromolecules* **2010**, *11*, 143.
[19] M. Hara, J. Wu, A. Lee, *Macromolecules* **1988**, *21*, 2214.
[20] B. K. Barai, R. S. Singhal, P. R. Kulkarni, *Carbohydr. Polym.* **1997**, *32*, 229.

[21] E. Kang, G. S. Jeong, Y. Y. Choi, K. H. Lee, A. Khademhosseini, S. H. Lee, *Nat. Mater.* **2011**, *10*, 877.
[22] E. Kang, Y. Y. Choi, S. K. Chae, J. H. Moon, J. Y. Chang, S. H. Lee, *Adv. Mater.* **2012**, *24*, 4271.
[23] K. H. Lee, S. J. Shin, Y. Park, S. H. Lee, *Small* **2009**, *5*, 1264.
[24] S. Mitragotri, J. Lahann, *Nat. Mater.* **2009**, *8*, 15.
[25] L. Leng, A. McAllister, B. Zhang, M. Radistic, A. Gunther, *Adv. Mater.* **2012**, *24*, 3650.
[26] A. S. Utada, E. Lorenceau, D. R. Link, P. D. Kaplan, H. A. Stone, D. A. Weitz, *Science* **2005**, *308*, 537.
[27] S. E. Chung, W. Park, S. Shin, S. A. Lee, S. Kwon, *Nat. Mater.* **2008**, *7*, 581.
[28] L. R. Snyder, J. J. Kirkland, *Introduction to Modern Liquid Chromatography*, 2nd ed, Wiley-VCH, New York **1979**, Ch. 6.
[29] A. L. Thangawng, P. B. Howell Jr., J. J. Richards, J. S. Erickson, F. S. Ligler, *Lab Chip* **2009**, *9*, 3126.
[30] W. J. Milliken, L. G. Leal, *J. Colloid Interface Sci.* **1994**, *166*, 275.
[31] D. Kiriya, M. Ikeda, H. Onoe, M. Takinoue, H. Komatsu, Y. Shimoyama, I. Hamachi, S. Takeuchi, *Angew. Chem. Int. Ed.* **2012**, *51*, 1553.
[32] A. W. Decho, *Carbohydr. Res.* **1999**, *315*, 330.
[33] M. O. Choi, Y. J. Kim, *Int. J. Biol. Macromol.* **2012**, *50*, 1188.
[34] N. S. Murthy, H. Minor, C. Bednarczyk, *Macromolecules* **1993**, *26*, 1712.
[35] Z. Zhang, M. Wan, Y. Wei, *Adv. Funct. Mater.* **2006**, *16*, 1100.
[36] Q. Wang, Y. Du, X. Hu, J. Yang, L. Fan, T. Feng, *J. Appl. Polym. Sci.* **2006**, *101*, 425.
[37] S. Y. Oh, D. I. Yoo, Y. Shin, H. C. Kim, H. Y. Kim, Y. S. Chung, W. H. Park, J. H. Youk, *Carbohydr. Res.* **2005**, *340*, 2376.
[38] N. Yuno-Ohta, M. Yamada, M. Inomata, H. Konagal, T. Kataoka, *J. Food Sci.* **2009**, *74*, E285.
[39] O. Hakimi, D. P. Knight, K. Vollrath, P. Vadgama, *Compos. B: Eng.* **2007**, *38*, 324.
[40] M. Tong, D. J. Browne, *Commun. Numer. Meth. Eng.* **2008**, *24*, 1171.
[41] A. Günther, K. F. Jensen, *Lab Chip* **2006**, *6*, 1487.